# Internal Ionization during Beta Decay*

PAUL STEPHAS
*Department of Physics, University of British Columbia, Vancouver, Canada*

AND

BERND CRASEMANN
*Department of Physics, University of Oregon, Eugene, Oregon*

(Received 19 June 1967)

In nuclear $\beta$ decay, atomic excitation, including ionization, can occur because of (i) imperfect overlap of parent and daughter orbital electron wave functions, and (ii) scattering of atomic electrons by the $\beta$ particle ("direct collisions"). In order to evaluate the relative importance of these two processes and test the possible role of nuclear matrix elements in orbital-electron ejection, published work on the subject has been reviewed. New measurements have been performed determining the total probability of $K$ ionization in the $\beta$ decay of $Tc^{99}$ [$(4.8\pm0.3)\times10^{-4}$ per $\beta$] and $Pm^{147}$ [$(9.3\pm1.4)\times10^{-5}$ per $\beta$]. The $K$ ionization probability as a function of $\beta$ energy has also been measured; a strong energy dependence is found, in disagreement with the traditional wave-function overlap theory. This theory is improved by including phase-space considerations, using relativistic electron wave functions in the calculation of the pertinent matrix elements, and paying careful attention to the antisymmetrization of the final-state wave function. The predictions of the modified wave-overlap theory agree very well with experiment. Direct collisions appear to play only a minor role. The calculations indicate that the ionization probability is inhibited in forbidden decay. A possible change in the shape factor for transitions accompanied by internal ionization is predicted.

## I. INTRODUCTION

IT has been realized for some time that a complete description of nuclear $\beta$ decay must include atomic variables in the specification of the initial and final states of the system undergoing the transition.[1,2] The atomic electrons affect $\beta$ decay rates only slightly in most cases, although there are notable exceptions among transitions of low end-point energy.[2,3] On the other hand, there is a measurable probability of atomic excitation and ionization during $\beta$ decay, in addition to the single ionization imposed by charge conservation in negative $\beta$ decay.

Two separate mechanisms can, in principle, account for *internal excitation* and *ionization*[4] during $\beta$ decay. These are: (i) the sudden change in nuclear charge and imperfect overlap of parent and daughter orbital electron wave functions, and (ii) scattering of atomic electrons by the $\beta$ particle ("direct collisions"). Subsequently, there can be additional ionization due to Auger and Coster-Kronig transitions.[5] These latter processes, however, occur *after* the $\beta$ decay and are not considered here.

In the present paper, the theory of internal ionization and excitation is reviewed, experiments on total internal ionization probability and internal ionization probability as a function of $\beta$-particle energy are described, and modifications of the imperfect wave-function overlap theory of internal ionization are suggested which bring it into accord with experiment.

## II. THEORY

### 1. Ionization due to Imperfect Orbital-Electron Wave-Function Overlap

Internal ionization can occur as a consequence of the sudden change in nuclear charge from $Z$ to $Z'=Z\pm1$ during $\beta$ decay. Only $\beta^-$ decay is considered here; the extension to positron decay is straightforward, and the electron-capture case has been treated elsewhere.[6-8] The eigenstates of the parent atom are no longer eigenstates of the daughter atom. As the electron cloud shrinks, adjustment can proceed adiabatically or by sudden transitions in which one or more electrons can go into excited states or into the continuum.

The rearrangement of the orbital electrons has been shown, both theoretically[9,10] and experimentally,[11-14] to occur as an integral part of the decay process and not as a subsequent step. One striking demonstration of this fact is based on the effect upon the $\beta$ spectrum of the total change in binding energy of the atom. The change in total binding energy increases with atomic number and reaches approximately 18 keV for $Z=90$.[1,10,15,16] If

* Work supported in part by the U. S. Atomic Energy Commission.

[1] P. Benoist-Gueutal, Ann. Phys. (Paris) 8, 593 (1953).
[2] J. N. Bahcall, Phys. Rev. 129, 2683 (1963).
[3] J. N. Bahcall, Phys. Rev. 124, 495 (1961).
[4] The term "internal ionization" is used in analogy with the names for other, similar effects related to nuclear decay, e.g., internal bremsstrahlung and internal conversion. Some authors refer to mechanism (i) as "shake-off".
[5] A. H. Snell, in *Alpha-, Beta-, and Gamma-Ray Spectroscopy*, edited by K. Siegbahn (North-Holland Publishing Company, Amsterdam, 1965), Vol. 2, Chap. XXV-B.
[6] H. Primakoff and F. T. Porter, Phys. Rev. 89, 930 (1953).
[7] J. G. Pengra and B. Crasemann, Phys. Rev. 131, 2642 (1963).
[8] R. L. Intemann and F. Pollock, Phys. Rev. 157, 41 (1967).
[9] H. M. Schwartz, Phys. Rev. 86, 195 (1952).
[10] R. Serber and H. S. Snyder, Phys. Rev. 87, 152 (1952).
[11] G. M. Insch, J. G. Balfour, and S. C. Curran, Phys. Rev. 85, 805 (1952).
[12] M. S. Freedman, F. Wagner, Jr., and D. W. Engelkemeir, Phys. Rev. 88, 1155 (1952).
[13] A. A. Jaffe and S. G. Cohen, Phys. Rev. 89, 454 (1953).
[14] E. Huster, Z. Physik 136, 303 (1953).
[15] L. Goldstein, J. Phys. Radium 8, 235 (1937).
[16] M. H. Hebb, Physica 5, 701 (1938).

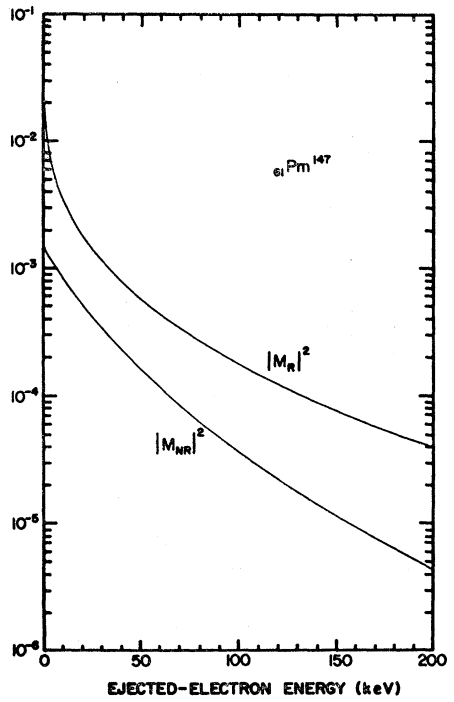


FIG. 1. Relativistic wave-function overlap $|M_R|^2$ [Eq. (9)] and nonrelativistic limit $|M_{NR}|^2$ [Eq. (10)] for 1$s$-electron ejection in the $\beta$ decay of $Pm^{147}$.

this energy were transferred to the $\beta$ particle *after* it has been emitted by the nucleus, then the entire $\beta$ spectrum would be shifted to higher energies without change in shape.[15,16] This shift would be clearly noticeable, in particular, in the low-energy decays of $Pb^{210}$ and $Pu^{241}$. However, no such shift has been observed.[11–14] It follows that the whole atom undergoes the transition in a single step, and atomic electron wave functions must be included, in addition to nuclear, $\beta$, and neutrino wave functions, in the matrix elements that determine the transition probability.

These concepts have been used[2,17] to describe internal ionization. The probability that an orbital electron, initially in state $\psi_i(Z,n)$, goes to a state $\psi_f(Z',n')$ due to the change in nuclear charge during $\beta$ decay is

$$w_{n'n}=2\pi|\langle\psi_f(\beta;Z',n')\psi_f(N)|H_\beta|\psi_\nu\psi_i(N)\psi_i(Z,n)\rangle|^2 \times\rho(\beta,\bar{\nu},e), \quad (1)$$

where $\psi_i(N)$ and $\psi_f(N)$ are the initial and final nuclear wave functions, $\psi_f(\beta;Z',n')$ is the antisymmetric final-state wave function for the $\beta$ particle and the ejected orbital electron, $\psi_\nu$ is the neutrino wave function, $H_\beta$ is the weak interaction Hamiltonian, and $\rho(\beta,\bar{\nu},e)$ is the density of final states for the $\beta$ particle, neutrino, and orbital electron. The units are such that $\hbar=c=m=1$. For allowed transitions, the nuclear, $\beta$, and neutrino contributions to the matrix element are independent of energy and the above expression can be factored[2,17,18]:

$$w_{n'n}=2\pi|\langle\psi_f(N)\psi_\beta|H_\beta|\psi_i(N)\psi_\nu\rangle|^2 \times|\langle\psi_f(Z',n')|\psi_i(Z,n)\rangle|^2\Xi\rho(\beta,\bar{\nu},e)$$
$$=w_\beta\frac{\rho(\beta,\bar{\nu},e)}{\rho(\beta,\bar{\nu})}\Xi|\langle\psi_f(Z',n')|\psi_i(Z,n)\rangle|^2, \quad (2)$$

where $w_\beta$ is the ordinary $\beta$-decay probability, $\rho(\beta,\bar{\nu})$ is the density of final states for a $\beta$ particle and a neutrino, and $\Xi$ is a factor which arises from the antisymmetrization of the final electron states. In writing Eqs. (2), it was assumed that the two final electrons do not Coulomb-interact; this approximation may be poor in cases where both electrons are slow.

On the grounds that the mean ejected-electron energy is generally small compared with the $\beta$ energy, Feinberg[17] neglected the ratio of statistical factors in the second of Eqs. (2) and set $\Xi$ equal to 2 to account for both $K$ electrons. The probability for internal ionization or excitation, per $\beta$ decay and per $K$ electron, then is

$$P_{n'n}\equiv w_{n'n}/w_\beta\cong 2|\langle\psi_f(Z',n')|\psi_i(Z,n)\rangle|^2. \quad (3)$$

This approach has been used by Goldstein,[19] and Migdal,[20] Feinberg,[17] Schwartz,[21] Levinger,[22] Winther,[23] and Green[24] to calculate the probability of internal ionization and excitation. Winther and Green used relatively exact wave functions for $He^6$ and $Kr^{85}$, respectively. The other authors have used nonrelativistic hydrogenic wave functions to describe the probability as a function of the nuclear charge $Z$.

We will calculate the wave-function overlap probability of Eq. (3) for a $K$ electron in the field of the parent nuclear charge $Z$ and a continuum electron in the field of the daughter nuclear charge $Z'$, using relativistic hydrogenic wave functions. The wave functions are of the form[25]

$$\psi=\begin{pmatrix} g(Z,r)\chi_\kappa^\mu \\ if(Z,r)\chi_{-\kappa}^\mu \end{pmatrix}, \quad (4)$$

where $\chi_{\pm\kappa}^\mu$ are the angular-momentum and spin-wave functions. The $K$-electron wave functions of the initial atomic state are

$$g(Z,r)=\frac{(2\zeta)^{\gamma+1/2}}{[2\Gamma(2\gamma+1)]^{1/2}}(1+\gamma)^{1/2}r^{\gamma-1}e^{-\zeta r},$$
$$f(Z,r)=-\left(\frac{1-\gamma}{1+\gamma}\right)^{1/2}g(Z,r), \quad (5)$$

[17] E. L. Feinberg, J. Phys. (U.S.S.R.) 4, 423 (1941).

[18] J. S. Levinger, J. Phys. Radium **16**, 556 (1955).
[19] L. Goldstein, J. Phys. Radium **8**, 316 (1937).
[20] A. Migdal, J. Phys. (U.S.S.R.) 4, 449 (1941).
[21] H. M. Schwartz, J. Chem. Phys. **21**, 45 (1953).
[22] J. S. Levinger, Phys. Rev. **90**, 11 (1953).
[23] A. Winther, Kgl. Danske Videnskab. Selskab, Mat. Fys. Medd. **27**, No. 2 (1952).
[24] A. E. S. Green, Phys. Rev. **107**, 1646 (1957).
[25] M. E. Rose, *Relativistic Electron Theory* (John Wiley & Sons, Inc., New York, 1961), Chap. V.

where $\zeta=\alpha Z$ and $\gamma^2=1-\zeta^2$, $\alpha$ being the fine-structure constant. The confluent hypergeometric continuum wave functions of the ejected electron are described by an integral representation

$$g(Z',r)=A+A^*,$$

$$f(Z',r)=i[p/(W+1)](A-A^*),$$

$$A=\frac{(W+1)^{1/2}p^{1/2}e^{\pi y/2}|\Gamma(\gamma'+iy)|e^{i\eta}(\gamma'+iy)}{2\pi^{3/2}(2pr)^{\gamma'+1}i^{2\gamma'+1}} \times\oint(u-\tfrac{1}{2})^{-\gamma'-1-iy}(u+\tfrac{1}{2})^{-\gamma'+iy}e^{2ipru}du, \quad (6)$$

where $W$ is the total energy of the electron, $W^2=p^2+1$, $\zeta'=\alpha Z'$, $\gamma'^2=1-\zeta'^2$, $\gamma'=\zeta'W/p$. The closed contour of integration contains the branch points at $u=\frac{1}{2}$ and $u=-1$.

We evaluate the wave-overlap integrals of Eq. (3) in the same manner as used by Sommerfeld in his treatment of the photoeffect.[17,22,26] A typical double integral such as

$$I=\int_0^\infty dr\, r^{2}r^{\gamma-1}e^{-\zeta r}\oint du\, r^{-\gamma'-1}(u-\tfrac{1}{2})^{-\gamma'-1+iy} \times(u+\tfrac{1}{2})^{-\gamma'-iy}e^{-2ipru} \quad (7)$$

is first integrated over the position variable $r$, with the result

$$I=\frac{\Gamma(1+\gamma-\gamma')}{(2ip)^{1+\gamma-\gamma'}}\oint du\frac{(u-\frac{1}{2})^{-\gamma'-1+iy}(u+\frac{1}{2})^{-\gamma'-iy}}{(u-i\zeta/2p)^{1+\gamma-\gamma'}}. \quad (8)$$

The quantity $\gamma-\gamma'$ is small; even for $Z$ as high as 80, its value is only $\sim5\times10^{-3}$. Therefore, we set $1+\gamma-\gamma'=1$ under the integral; this is the only approximation made in the calculation. The contour is now transformed to infinity and the integral evaluated by taking the residue at the simple pole at $u=i\zeta/2p$.

After some long but straightforward algebraic manipulations, one obtains

$$|M_R|^2\equiv|\langle\psi_f(Z',W)|\psi_i(Z,K)\rangle|^2 =\frac{2^{4\gamma'}\zeta^{1+2\gamma}[\Gamma(1+\gamma-\gamma')]^2}{\pi\Gamma(2\gamma+1)}\frac{e^{\pi y}|\Gamma(\gamma'+iy)|^2}{p^{3+2\gamma-4\gamma'}(p^2+\zeta^2)^{2+2\gamma'}} \times\exp[-4y\tan^{-1}(p/\zeta)]\{(W+\gamma)(p^2+\zeta^2)(p^2+\zeta'^2) -[2p^2\zeta\zeta'(\gamma'+W)+(p^2-\zeta^2)(p^2\gamma'-\zeta'^2W)] \times[(1+\gamma W)\cos\delta+p\zeta\sin\delta] -[2\zeta(p^2\gamma'-\zeta'^2W)-\zeta'(p^2-\zeta^2)(\gamma'+W)] \times[p(1+\gamma W)\sin\delta-p^2\zeta\cos\delta]\}, \quad (9)$$

[26] H. A. Bethe and E. E. Salpeter, in *Handbuch der Physik*, edited by S. Flügge (Springer Verlag, Berlin, 1957), Vol. XXXV.

TABLE I. Antisymmetrization factor $\Xi$ and shape factor $S(W_\beta,W_\nu)$ for various types of transitions accompanied by internal ionization.

| Isotope | Type of decay | $S(W_\beta,W_\nu)$[a] | $\Xi$ |
|---|---|---|---|
| | allowed | 1 | $\frac{1}{2}$ |
| $Pm^{147}$ | 1st forbidden, nonunique | 1 | $\frac{1}{4}$ |
| $Y^{90}$ | 1st forbidden, unique | $W_\nu^2+\frac{1}{2}(W_\beta^2-1)$ | $\frac{1}{4}$ |
| $Tc^{99}$ | 2nd forbidden, nonunique | $W_\nu^2+0.42(W_\beta^2-1)$ | $\approx\frac{1}{2}$ |

[a] $W_\nu=W_K-W_\beta-W$.

where $\delta=(\gamma-\gamma')\pi$. The nonrelativistic limit, obtained in the usual way by letting $W=1$ and $\gamma=\gamma'=1$, is

$$|M_{NR}|^2=\frac{2^6\zeta^5\zeta'}{Z^2(p^2+\zeta^2)^4}\frac{\exp[-4y\tan^{-1}(p/\zeta)]}{1-\exp(-2\pi y)}; \quad (10)$$

this expression agrees with previous results[17,20,22,6] obtained from nonrelativistic wave functions.

Equations (9) and (10) are plotted in Fig. 1 for $Pm^{147}$. The relativistic wave-function overlap probability exceeds the result of the nonrelativistic approximation at all energies, even in the low-energy "nonrelativistic" region, and has a smaller slope above $\sim20$ keV ejected-electron energy. Only for very low $Z$ are the relativistic and nonrelativistic results comparable. It is apparent that the predicted $K$-ionization probability decreases rapidly with increasing energy of the ejected electron, but does not vanish at the end-point energy of the $\beta$ spectrum. This nonphysical result of the theory was attributed by Levinger to the use of the sudden approximation.[18]

As can be seen from Eq. (3), the total probability, per decay, for ejection of a $K$ electron is obtained by integrating Eq. (10) over ejected-electron energy [Eq. (9) is weakly singular at $W=1$]:

$$P_K\cong a_KZ^{-2}. \quad (11)$$

The coefficient $a_K$ is computed as $\sim0.6$, and the mean energy of the ejected electrons is found to be approximately equal to the ionization energy of the $K$ shell.[17,22] For medium $Z$, the $K$ ionization probability is of the order of $10^{-4}$ per $\beta$ decay.

### 2. β-Energy Dependence of Internal Ionization Probability

The imperfect wave-function overlap formalism outlined in the preceding section predicts no dependence of the $K$ ionization probability during $\beta$ decay on the energy of the emitted $\beta$ particle. The experiments described in Sec. III 3 below do, however, show that this probability is in fact strongly $\beta$-energy-dependent. At first glance, the experimental results may lead one to suspect that the direct interaction mechanism, which is

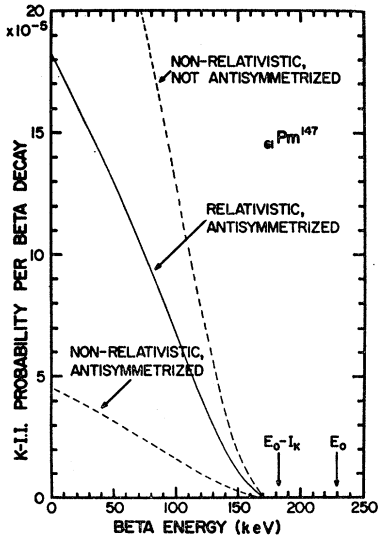


FIG. 2. $K$-shell internal ionization probability per $\beta$ decay of $Pm^{147}$, as a function of $\beta$-particle energy. The effect of using relativistic wave functions to calculate the transition matrix elements and of antisymmetrizing the final-state wave function is indicated.

$\beta$-energy-dependent (Sec. II 4), dominates the internal ionization process. But on the other hand, total ionization probabilities agree well with the $Z^{-2}$ law of Eq. (11) (Sec. III 2$B$), making it appear unlikely that direct collisions should provide the dominant mechanism for bound-electron ejection. We have therefore reexamined the imperfect wave-function overlap theory; in this section, phase-space arguments are included in the theory that lead to the prediction of $\beta$-energy-dependent ionization probabilities.

In the conventional theory,[17] the ratio of statistical factors in Eq. (2) is neglected because the mean energy of the ejected orbital electrons is low, of the order of the $K$-shell binding energy for $1s$ electrons. However, this approximation is not valid for decays with low $\beta$ endpoint energies and for the internal ionization probability associated with the emission of low-energy $\beta$ particles.

Consider a $\beta$ decay which, for generality, involves energy-dependent nuclear matrix elements. The matrix elements can be factored into two parts, an energy-independent factor $|M_N|^2$ and a shape factor $S_\beta(W_\beta,W_\nu)$ which depends on the total energies $W_\beta$ and $W_\nu$ of the $\beta$ particle and neutrino. After integrating over the neutrino energies, we have

$$|\langle\psi_f(N)\psi_\beta|H_\beta|\psi_i(N)\psi_\nu\rangle|^2 = |M_N|^2 S_\beta(W_\beta, W_0-W_\beta). \quad (12)$$

Similarly, retaining the statistical factors in Eq. (2) and integrating over neutrino energies, we find for the $K$-shell ionization probability as a function of $\beta$ energy and ejected-electron energy

$$dw_K(W_\beta,W) = 2^3(2\pi)^{-5}|M_N|^2 S(W_\beta, W_K-W_\beta-W) \times|\langle\psi_f(Z',W)|\psi_i(f,K)\rangle|^2\Xi \times(W_K-W_\beta-W)^2 p_\beta W_\beta dW_\beta pW dW, \quad (13)$$

where $W_K$ stands for the maximum total relativistic energy (including the rest energy of two electrons) available for $K$-electron ejection, i.e., $W_K=W_0+1-I_K'$. The shape factor $S$ will in general be different from $S_\beta$ as determined by the summation over the final antisymmetrized electron states; however, we assume that $|M_N|^2$ is the same as for ordinary $\beta$ decay. Our calculated values of $S$ and $\Xi$ for various types of $\beta$ decay are given in Table I. For the second forbidden, nonunique case, a definite value for $\Xi$ could not be obtained without detailed knowledge of the relative magnitude of the various $\beta$ decay matrix elements; in our computations, we assume that $S$ has the same form as $S_\beta$, the latter being determined experimentally.

It follows from Eq. (13) that the $K$-shell ionization probability *per decay*, as a function of $\beta$ energy, is

$$P_K(W_\beta)=[2\pi^2(W_0-W_\beta)^2 S_\beta(W_\beta, W_0-W_\beta)]^{-1}\Xi \times\int_1^{W_K-W_\beta} dW\,(W_K-W_\beta-W)^2 pW|M|^2 \times S(W_\beta, W_K-W_\beta-W), \quad (14)$$

where $|M|^2$ is given by either Eqs. (9) or (10). A

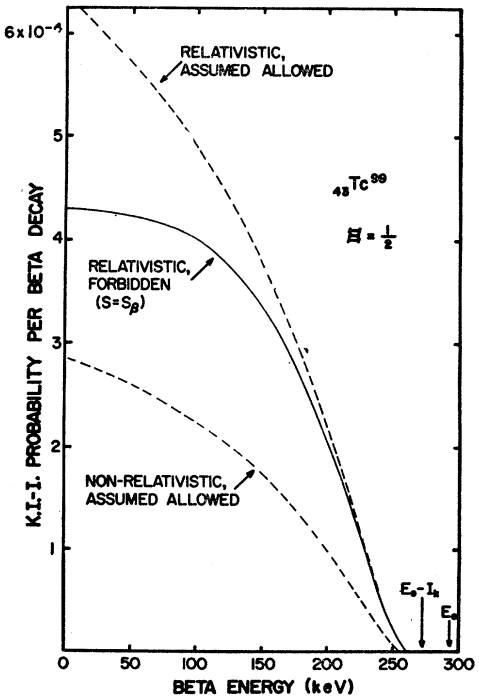


FIG. 3. $K$-shell internal ionization probability for $Tc^{99}$, per $\beta$ decay. Inclusion of the forbidden shape factor $S_\beta$ reduces the predicted ionization probability.

graph of this expression applied for $Pm^{147}$, using both relativistic and nonrelativistic wave functions, is shown in Fig. 2. The results of the nonrelativistic calculation are shown, both without antisymmetrization of the final-state wave function ($\Xi=2$) and with antisymmetrization (see Table I for values of $\Xi$). It will be shown in Sec. III 3 that neither nonrelativistic form agrees with experiment, while the antisymmetrized relativistic result is in excellent agreement with the data.

The internal ionization probability per $\beta$ is inhibited in forbidden $\beta$ decay, as compared with allowed transitions. This is illustrated for $Tc^{99}$ in Fig. 3, where $\Xi$ is taken to be $\frac{1}{2}$. It can be seen from Figs. 2 and 3 that for low $\beta$ end-point energy transitions, the internal ionization probability per decay varies strongly with $\beta$-particle energy. On the other hand, this variation need not be large (except near the end-point) in transitions with high $\beta$ end-point energy. This is shown, for example, by the upper curve in Fig. 4, which represents the internal ionization probability for $Y^{90}$, calculated with nonrelativistic wave functions treating the (actually unique first-forbidden) transition as allowed. A similarly slight $\beta$-energy dependence of the internal ionization probability is found when relativistic wave functions are used, and even for forbidden transitions, as long as the shape factor $S$ has the same form as $S_\beta$, so that the approximation inherent in Eq. (3) is relatively good within a factor of $2\Xi$. However, an internal ionization-modified shape factor can produce a strong $\beta$-energy dependence of the internal ionization probability even when the end-point energy is high; this is illustrated by the lower curve in Fig. 4.

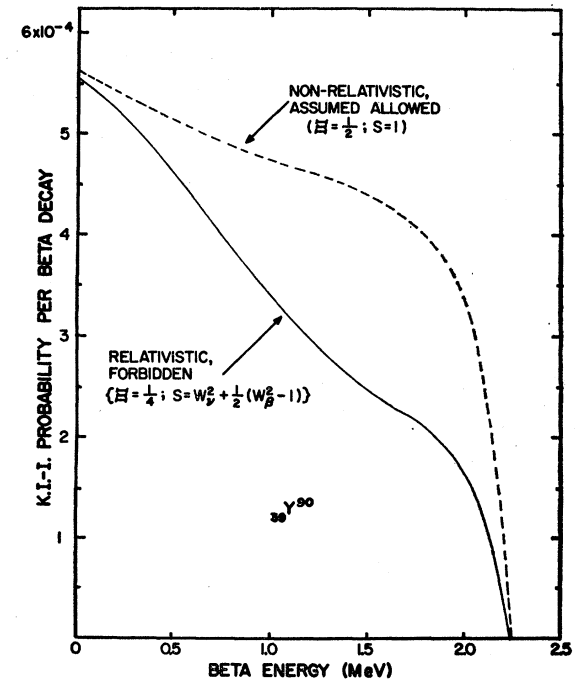


FIG. 4. $K$-shell internal ionization probability for $Y^{90}$, per decay. The shape factor $S$ introduces a strong $\beta$-energy dependence of the ionization probability.

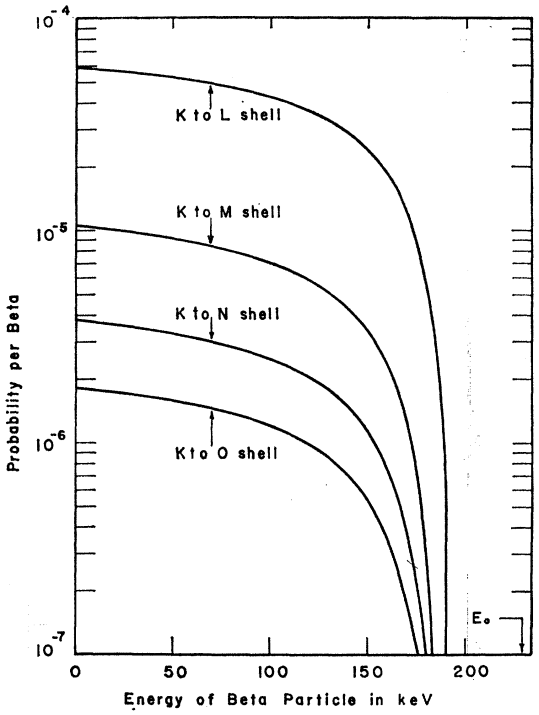


FIG. 5. Probability, per $\beta$ decay, of internal excitation of the $K$ shell of $Pm^{147}$, as a function of $\beta$-particle energy.

### 3. Internal Excitation due to Imperfect Orbital-Electron Wave-Function Overlap

The probability for excitation, due to the change in nuclear charge during $\beta$ decay, of an atomic electron from an initial state with principal quantum number $n$ to a final state $n'$ (assumed previously vacant) follows from Eq. (1):

$$dw_{n'n}=2\pi|M_N|^2S(W_\beta,W_\nu)|\langle\psi_f(Z',n')|\psi_i(Z,n)\rangle|^2 \times d^3p_\beta d^3p_\nu(2\pi)^{-6}\delta(W_{n'n}-W_\beta-W_\nu). \quad (15)$$

Here, $W_{n'n}$ stands for $W_0+I_{n'}-I_n$, where $I_n$ and $I_{n'}$ are the ionization energies of the states $n$ and $n'$, respectively. For hydrogenic wave functions, the transitions are subject to the selection rules $\Delta l=0$ and $\Delta m=0$. It has been shown[19–22] that the atomic matrix element for nonrelativistic hydrogenic wave functions has the form

$$|\langle\psi_f(Z',n')|\psi_i(Z,n)\rangle|^2=a_{n'n}Z^{-2}, \quad n'\neq n. \quad (16)$$

Values of some of the imperfect wave-overlap coefficients $a_{n'n}$ have been computed by Schwartz[21] and others. The internal excitation probability per decay, as a function of $\beta$ energy, then is

$$P_{n'n}(W_\beta)=\frac{a_{n'n}}{Z^2}\frac{(W_{n'n}-W_\beta)^2S(W_\beta,W_{n'n}-W_\beta)}{(W_0-W_\beta)^2S(W_\beta,W_0-W_\beta)}. \quad (17)$$

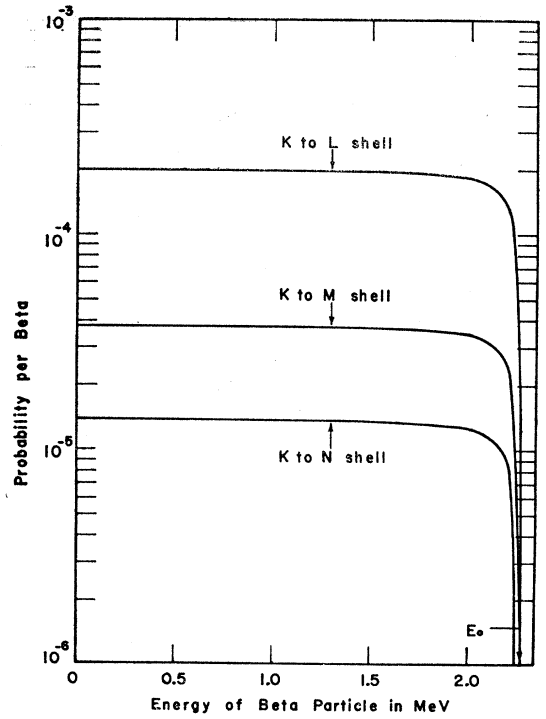


FIG. 6. Probability, per $\beta$ decay, of internal excitation of the $K$ shell of $Y^{90}$, as a function of $\beta$-particle energy.

In these equations, $Z$ is not necessarily the nuclear charge, but rather the effective charge for a particular orbital. Since the lowest-$n$ states are normally occupied, internal excitation of $K$ electrons most likely leads to high-$n$ states or to the continuum. Transitions of $K$ electrons to all bound states above the $M$ shell are no more than 15% as probable as transitions to the continuum.

Figures 5 and 6 show internal excitation probability as a function of $\beta$ energy, for $Pm^{147}$ and $Y^{90}$, respectively. As for internal ionization, the probability per decay is relatively constant over most of the $\beta$ energy range for isotopes with high $\beta$ end-point energy, such as $Y^{90}$, but not for isotopes with low end-point energy, e.g., $Pm^{147}$.

### 4. Ionization due to Direct Collision

In the "direct collision" mechanism of internal ionization, the $\beta$ particle scatters an initially bound orbital electron through the Coulomb interaction. The theory of this process was first developed by Feinberg.[17,27] Through first-order perturbation theory, the $K$-shell ionization probability can be written

$$dw_K(E,W_j,W_\beta)=2\pi|M|^2\rho(\beta,e)\,, \qquad (18)$$

where $W_j$ is the initial and $W_\beta$ the final energy of the $\beta$ particle, $E$ is the nonrelativistic kinetic energy of the ejected orbital electron, and the matrix element $M$ is

$$|M|=|\langle\psi_f(Z,E)\psi_\beta(W_\beta)|\frac{\alpha}{r}|\psi_i(Z,K)\psi_\beta(W_j)\rangle|\,. \qquad (19)$$

Here, $\psi_i(Z,K)$ is the $1s$ atomic wave function. In his "semirelativistic" calculation, Feinberg describes the initial $\beta$ particle by an outgoing spherical wave, and both final electrons by plane waves, the $\beta$ particle being treated relativistically with energy $W_\beta^2=p_\beta^2+1$ and the ejected electron being treated nonrelativistically with energy $E=p^2/2\ll W_\beta$. The result is

$$|M|=\frac{16\pi^2\alpha^2\zeta^3W_\beta}{p_\beta^3p^4}\frac{1}{p^2\cos^2\theta+\zeta^2}\,, \qquad (20)$$

where $\zeta=\alpha Z$, $I_K=\frac{1}{2}\zeta^2$, and $\theta$ is the angle subtended by the two final electrons. It follows that the direct-collision ionization probability is

$$dw_K(W_\beta,E)=4\alpha^2\pi^{-1}I_K\tan^{-1}(E/I_K)^{1/2}\times\frac{W_\beta(W_\beta-E-I_K)}{(W_\beta-E-I_K)^2-1}E^{-2}dE. \qquad (21)$$

With the approximations $W_\beta\gg E\gg I_K$, this result is reduced to

$$dw_K(W_\beta,E)=2\alpha^2I_KW_\beta^2(W_\beta^2-1)^{-1}E^{-2}dE. \qquad (22)$$

From this approach, we have computed the direct-

TABLE II. Probabilities of internal ionization and excitation of the $K$ shell.

| Isotope | Probability (per $\beta$) | References |
|---|---|---|
| $He^6$ | $0.101\pm0.002$ | a |
| $P^{32}$ | $4.7\times10^{-3}$ | b,c |
| | $9.9\times10^{-3}$ | d–f |
| $S^{35}$ | $(2.3\pm0.7)\times10^{-3}$ | g |
| | $1.7\times10^{-3}$ | d,h |
| $Sr^{90}$-$Y^{90}$ | $(13.1\pm1.5)\times10^{-3}$ | i |
| | $5.8\times10^{-4}$ | c |
| $Y^{90}$ | $4.75\times10^{-4}$ | b |
| | $(3.2\pm0.3)\times10^{-4}$ | j,k |
| $Tc^{99}$ | $(4.8\pm0.3)\times10^{-4}$ | k |
| | $(4.1\pm0.3)\times10^{-4}$ | j,k |
| $Pr^{143}$ | $(4.25\pm0.85)\times10^{-4}$ | l |
| $Pm^{147}$ | $(3.85\pm0.5)\times10^{-4}$ | m |
| | $(1.30\pm0.26)\times10^{-4}$ | l |
| | $(8\pm8)\times10^{-5}$ | n |
| | $(9.3\pm1.4)\times10^{-5}$ | k |
| | $(5.1\pm0.5)\times10^{-5}$ | j,k |
| $Bi^{210}$ | $(1.2\pm0.5)\times10^{-4}$ | n |
| | $(1.3\pm0.2)\times10^{-4}$ | i |

[a] Reference 41.
[b] Reference 46.
[c] G.-A. Renard, J. Phys. Radium **16**, 575 (1955).
[d] Determined by coincidence measurements.
[e] Reference 42.
[f] G. Charpak, J. Phys Radium **16**, 567 (1955).
[g] W. Rubinson and J. J. Howland, Jr., Phys. Rev. **96**, 1610 (1954).
[h] Reference 43.
[i] A. Michalowicz and R. Bouchez, J. Phys. Radium **16**, 578 (1955).
[j] Determined by coincidence measurements, see Sec. III 3.
[k] Present work.
[l] H. Langevin-Joliot, Ann. Phys. (Paris) **2**, 16 (1957).
[m] F. Boehm and C. S. Wu, Phys. Rev. **93**, 518 (1954).
[n] Reference 44.

[27] E. L. Feinberg, Yadern. Fiz. **1**, 612 (1965) [English transl.: Soviet J. Nucl. Phys. **1**, 438 (1965)].

TABLE III. Probabilities of internal ionization and excitation in various shells.

| Isotope | Shell | Probability (per $\beta$) | References |
|---|---|---|---|
| $He^6$ | $2K^a$ | $(1.8\pm1.5)\times10^{-4}$ | b |
| $Sr^{90}$-$Y^{90}$ | $L$ | $5\times10^{-4}$ | c |
| $Y^{90}$ | $L$ | $6.0\times10^{-3}$ | d |
| $Pr^{143}$ | $L$ | $(1.9\pm0.2)\times10^{-3}$ | e,f |
| $Pm^{147}$ | $L$ | $(2.05\pm0.3)\times10^{-3}$ | g |
| | $L$ | $(1.7\pm0.1)\times10^{-3}$ | e,h |
| $Bi^{210}$ | $L$ | $(6\pm3)\times10^{-4}$ | g |
| | $L$ | $\approx5\times10^{-4}$ | i |
| | $L$ | $9.1\times10^{-4}$ | c |
| | $M$ | $2.9\times10^{-3}$ | c |

[a] Double ionization of the $K$ shell.
[b] Reference 41.
[c] G.-A. Renard, J. Phys. Radium **16**, 575 (1955).
[d] Reference 46.
[e] Measurement by coincidence techniques.
[f] Reference 45.
[g] F. Boehm and C. S. Wu, Phys. Rev. **93**, 518 (1954).
[h] Reference 44.
[i] A. Michalowicz and R. Bouchez, J. Phys. Radium **16**, 578 (1955).

collision internal-ionization probabilities for $Pm^{147}$ and $Tc^{99}$, as functions of $\beta$ energy; the results are shown in Fig. 7.

The contribution of the direct-collision (DC) mechanism in internal ionization has generally been considered negligible as compared with the imperfect wave-function overlap ($\Delta Z$) mechanism. From a comparison of matrix elements, the relative importance of the two processes has been estimated[17] as

$$\frac{P_{DC}}{P_{\Delta Z}}\cong\frac{|M_{DC}|^2}{|M_{\Delta Z}|^2}\cong\frac{I_K}{E_\beta}, \tag{23}$$

which is generally much less than unity. However, Feinberg has recently pointed out that this ratio may not be less than unity for nuclei with high $Z$ and low decay energies.[27] Comparison of Fig. 7 with Fig. 3 shows that the direct-collision process is less probable for high energies, but not necessarily at low energies, where the calculations are not very accurate.

In a recent paper,[28] Weiner has reexamined the theory of the direct-collision mechanism of internal ionization. A semiphenomenological method is employed, based on experimental electron impact cross sections from which the contribution of "glancing collisions" ("photoeffect" collisions that correspond to large impact parameters) has been subtracted with the aid of the Weizsäcker-Williams method. Total internal ionization probabilities derived from this approach are compared with experimental values in Sec. III 2$B$ below; large discrepancies are found.

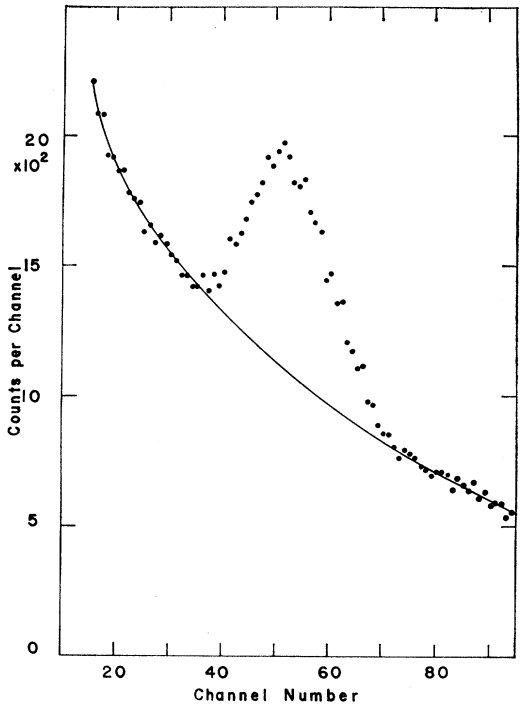


FIG. 8. Typical photon spectrum from a $Tc^{99}$ source. The peak is produced by 19.6-keV Ru $K$ x rays, superimposed on a bremsstrahlung continuum.

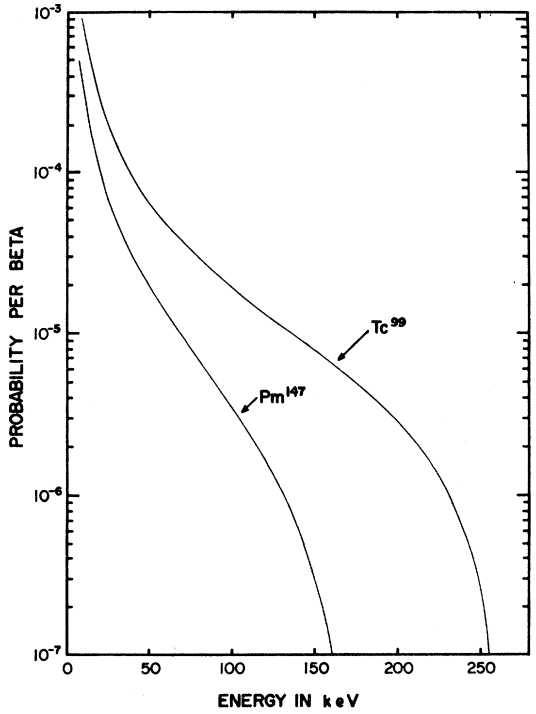


FIG. 7. Probability, per $\beta$ decay, of internal ionization of the $K$ shell of $Pm^{147}$ and $Tc^{99}$ by the "direct-collision" mechanism, as a function of $\beta$-particle energy.

## III. EXPERIMENTAL TESTS

Verification of theoretical predictions regarding $K$-shell internal ionization and excitation during $\beta$

[28] R. M. Weiner, Phys. Rev. **144**, 127 (1966).

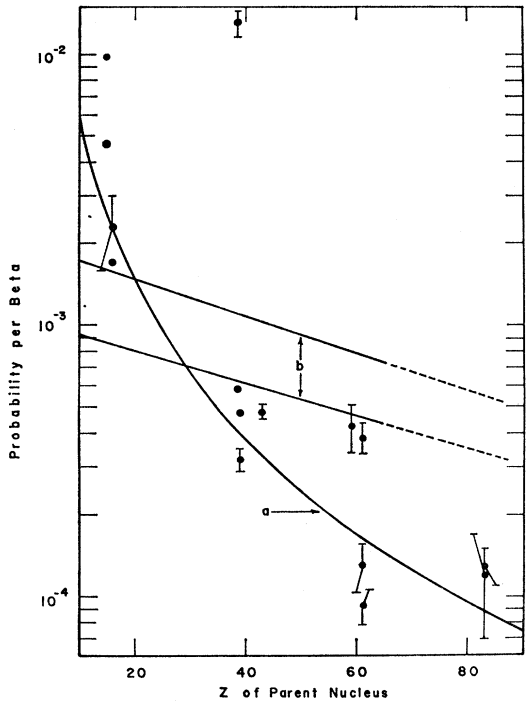


FIG. 9. Total probability, per $\beta$ decay, of internal excitation and ionization of the $K$ shell, as a function of atomic number. Experimental values are those listed in Table II. Theoretical curve a represents the prediction of the simple wave-function overlap theory [Eq. (11)]: $P_K=0.6Z^{-2}$. Curves b indicate the approximate limits of the probability predicted by the "direct-collision" theory, according to Ref. 28.

decay must be based on measurements of the electron spectrum and of electron–x-ray and electron-electron coincidences. Direct measurements of the charge of the final atom do not yield accurate information on the $K$ shell ionization probability[24] since the final charge is affected by ionization of all shells and by a complicated cascade of Auger and Coster-Kronig transitions, for which theoretical predictions are only semiquantitative.

### 1. Electron Spectrum

The spectrum of ejected orbital electrons rises sharply with decreasing energy. Therefore, it can in principle be distinguished from the ordinary $\beta$ distribution, although this has not yet been accomplished. Excessive low-energy electrons have been reported[29] in spectra that had been carefully corrected for instrumental effects including backscattering from the source support. However, Kurie plots of these spectra could be straightened out by a shape factor $(1+b/W, 0.2<b<0.4)$ which also straightened the positron spectrum of $Na^{22}$, so that the observed excess of low-energy electrons cannot be ascribed to internal ionization.[2,30]

[29] O. E. Johnson, R. G. Johnson, and L. M. Langer, Phys. Rev. **112**, 2004 (1958).
[30] J. H. Hamilton, L. M. Langer, and W. G. Smith, Phys. Rev. **112**, 2010 (1958).

Detection of ejected orbital electrons accompanying positron decay is more feasible, since separation of electrons and positrons by magnetic deflection[31] can be employed. An early report[32] of rather abundant electrons accompanying the positron spectrum of $Sc^{44}$ was later contradicted.[33] But Hamilton, Langer, and Smith[30] measured the electron distribution associated with the positron spectrum of $Na^{22}$ and found $N_e/N_{e^+}=(4.3_{-2.4}^{+1.4})\times10^{-2}$, in reasonable agreement with the simple imperfect wave-function overlap theory for the $K$ and $L$ shells, although the distribution did not decrease as rapidly with increasing electron energy as predicted by that theory.

### 2. Measurements of Internal Ionization and Excitation Probability by X-Ray Detection

#### *A. Determination of K-Shell Internal Ionization and Excitation Probability in $Tc^{99}$ and $Pm^{147}$ Decay*

In isotopes which $\beta$-decay exclusively to the ground state of the daughter nucleus, the detection of characteristic x rays superimposed on the internal and external bremsstrahlung continuum provides a straightforward method for measuring the internal ionization and excitation probability. We have measured $K$-shell ionization and excitation probabilities in the decay of $Tc^{99}$ and $Pm^{147}$ by using a scintillation counter to detect the photon spectrum. The detector consisted of a 25-mm-diam, 5-mm-thick Harshaw NaI(Tl) crystal covered with a 0.013-mm Be window and coupled to a selected Phillips XP1010 photomultiplier tube; this device resolved the 5.9-keV Mn $K$ x ray from noise with a peak-to-valley ratio of 25. Spectra were recorded with a 512-channel analyzer.

Source materials were obtained from the Oak Ridge

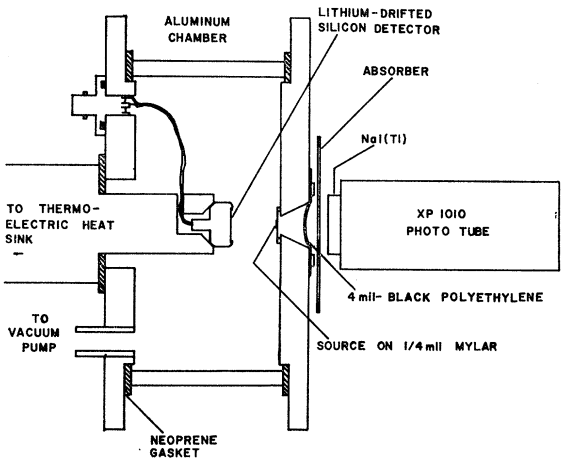


FIG. 10. Cross section of apparatus for measurement of internal excitation and ionization probabilities.

[31] B. Crasemann, Rev. Sci. Instr. **24**, 470 (1953).
[32] J. A. Bruner, Phys. Rev. **84**, 282 (1951).
[33] J. W. Blue and E. Bleuler, Phys. Rev. **100**, 1324 (1955).

National Laboratory in the form of $NH_4TcO_4$ in water and $PmCl_3$ in HCl. Sources were prepared by evaporating drops of radioactive solution on 0.00025-in. aluminized Mylar and were visually inspected for uniformity. To make certain that only a negligible number of $K$ x rays was produced by fluorescence, series of sources of decreasing thickness were prepared and measured, until the number of $K$ x rays per $\beta$ decay no longer decreased. The final experiments were carried out with a 180-$\mu$g/cm$^2$ $Tc^{99}$ source and a 1-$\mu$g/cm$^2$ $Pm^{147}$ source.

Various thicknesses of Plexiglas or Tenite[34] were used as electron absorbers, depending on $\beta$ energy. The x-ray attenuation coefficients for Plexiglas were taken from the literature,[35] while those for the low-density plastic Tenite were determined experimentally.[36]

The probability per $\beta$ decay of forming a hole in the $K$ shell is given by

$$P_K = N_K(1+g)/N_0\omega_K a\epsilon, \qquad (24)$$

where $N_0$ is the total number of $\beta$-decay events, $N_K$ is the number of $K$ x-ray counts in the photopeak of the photon (scintillation) spectrum, $\omega_K$ is the $K$-shell fluorescence yield,[37] $a$ is the $K$ x-ray attenuation correction for the electron absorber and the beryllium window, $\epsilon$ is the detector efficiency (including solid angle), and $g$ is the escape-peak correction. The solid angles subtended by the detector were calculated from equations pertinent to small source-to-detector distances.[38,39] The escape-peak correction $g$, defined as the number of counts in the escape peak divided by the number of counts in the photopeak, is zero for $Tc^{99}$ and[40] $\sim$0.24 for $Pm^{147}$.

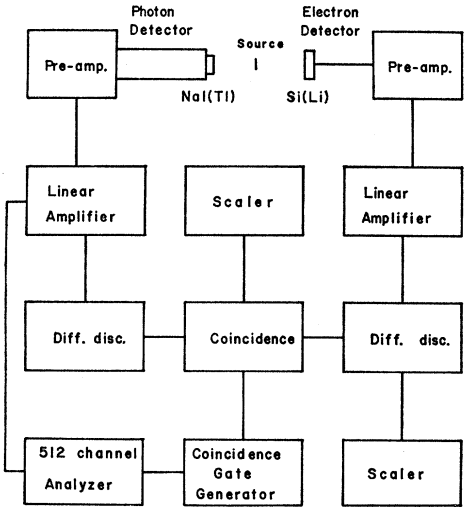


FIG. 11. Block diagram of electronics for measurement of internal excitation and ionization probabilities.

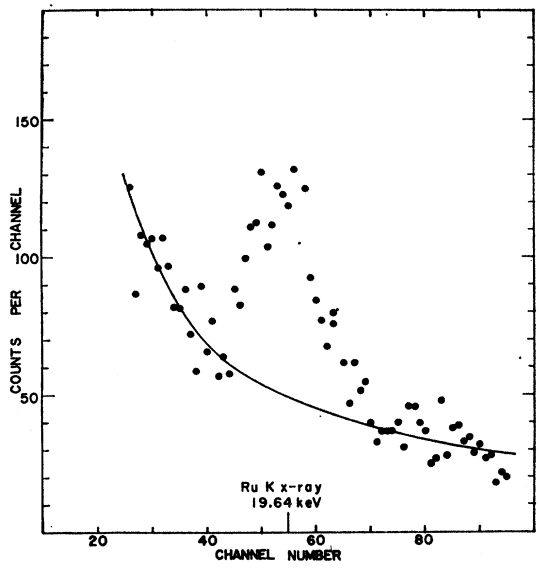


FIG. 12. Typical spectrum of photons from a $Tc^{99}$ source, observed in coincidence with $\beta$ particles between 112- and 143-keV energy, during 16 000-min live time.

A typical photon spectrum is shown in Fig. 8. The bremsstrahlung continuum under the peak was estimated by interpolation between adjoining energy regions. From three separate runs for each isotope, the following values have been found for the $K$-shell internal ionization and excitation probability per $\beta$ decay:

$$Tc^{99}: \quad P_K = (4.8\pm0.3)\times10^{-4},$$
$$Pm^{147}: \quad P_K = (9.3\pm1.4)\times10^{-5}.$$

### *B. Summary of Available Data on Internal Ionization and Excitation Probabilities*

The probabilities of internal ionization and excitation of the $K$ shell of various isotopes during $\beta$ decay, measured by different experimenters, are collected in Table II. For completeness, we list in Table III the measured probabilities for other shells and, in one case, for double ionization of the $K$ shell. Indicated errors have been quoted from the original papers.

The $He^6$ data[41] were obtained by measuring the charge of the daughter atom after $\beta$ decay; they are in excellent agreement with theoretical values[23] of $0.105\pm0.015$ and $<10^{-3}$ for the singly and doubly ionized $K$ shell, respectively, based on the simple imperfect wave-overlap formalism. All other experiments required the extraction of the x-ray peak of the daughter atom from a continuum and sometimes from spurious x rays. Except where coincidence techniques

[34] Eastman Chemical Products, Inc., Kingsport, Tennessee.
[35] P. Venugopala Rao and B. Crasemann, Phys. Rev. 137, B64 (1965).
[36] P. Stephas, Ph.D. thesis, University of Oregon, 1966 (unpublished).
[37] G. J. Nijgh, A. H. Wapstra, and R. Van Lieshout, *Nuclear Spectroscopy Tables* (North-Holland Publishing Company, Amsterdam, 1959).
[38] B. P. Burtt, Nucleonics 5, 28 (August, 1949).
[39] C. Oldano and A. Pasquarelli, Nucl. Instr. Methods 36, 192 (1965).
[40] P. Venugopala Rao (private communication).
[41] T. A. Carlson, F. Pleasanton, and C. H. Johnson, Phys. Rev. 129, 2220 (1963).

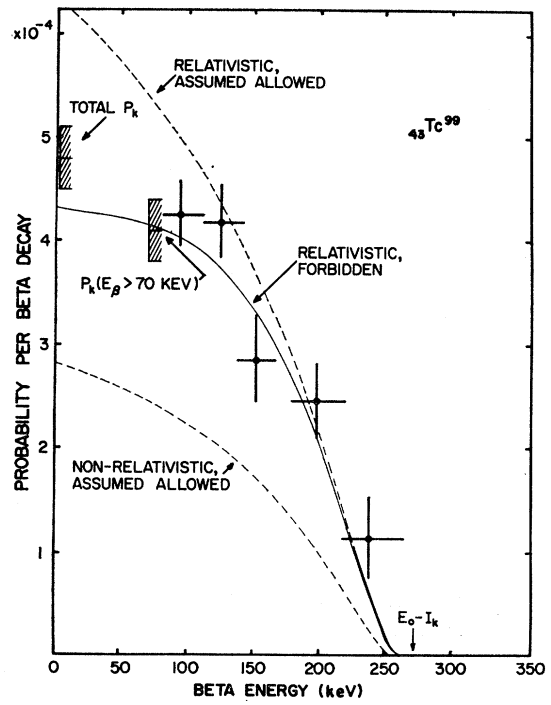


FIG. 13. Measured $K$-shell internal excitation and ionization probability in the $\beta$ decay of $Tc^{99}$, as a function of $\beta$-particle energy. Horizontal bars indicate extent of $\beta$-energy window in each coincidence measurement. Vertical bars represent standard deviations. Cross-hatched vertical bars indicate measured total $K$-shell excitation and ionization probability associated with emission of $\beta$ particles above given energy. Curves are $K$-shell internal ionization probabilities calculated according to the modified imperfect wave-function overlap theory (Sec. II 2), all computed with antisymmetrized final-state wave functions ($\Xi=\frac{1}{2}$). A good quantitative fit is obtained if relativistic wave functions are used in the transition matrix element and the final-state wave function is antisymmetrized.

were used, absolute source strengths had to be determined. In view of the difficulty of measuring these very low probabilities, agreement within a factor of 2 or 3 between the results from various laboratories may be considered good. On the other hand, attention is called to the discrepancy by a factor of 20 between results reported for the $K$ ionization probability in $Sr^{90}$-$Y^{90}$.

In Fig. 9, the measured $K$-shell internal ionization and excitation probabilities are compared with theory. It is seen that the dependence on atomic number is very nearly that predicted by the simple imperfect wave-function overlap theory [Eq. (11)], $P_K=0.6Z^{-2}$. On the other hand, the direct-collision mechanism after the theory of Weiner[28] leads to a predicted $Z$ dependence that is very much at variance with the measured probabilities.

### 3. Internal Ionization Probability as a Function of β Energy: K-X-Ray–Electron Coincidence Measurements

Coincidence measurements between x rays and electrons can provide a more sensitive test of the theory of internal ionization than is obtainable from simple x-ray intensity measurements, since the dependence of excitation and ionization probability on $\beta$ energy can be established. Moreover, coincidence experiments have the advantage that the absolute source strength need not be known and the photon continuum is less intense. On the other hand, the coincidence counting rate is very low, since weak sources must be employed to minimize fluorescence.

Coincidences between $K$ x rays and all electrons above a given, fixed threshold (10–14 keV) have been measured by Charpak and Suzor.[42–45] The shape of the electron spectrum in coincidence with x rays emitted during $\beta$ decay has not yet been measured in any case; this would provide a further critical test of theoretical predictions.

Through the experiments described in the present section, we have determined the $K$-shell excitation and ionization probability of $Tc^{99}$ and $Pm^{147}$ as a function of $\beta$-particle energy, by observing the photon spectrum in coincidence with various segments of the $\beta$ spectrum. Figure 10 shows the apparatus. The scintillation counter described in Sec. III 2$A$ served as x-ray detector. Electrons were observed with a T.M.C. lithium-drifted silicon detector of 110-mm² active area and 2-mm depletion depth, operated in a vacuum and cooled to −10°C by a thermoelectric heat sink. The source was mounted in the vacuum chamber, with the 0.00025-in. Mylar source backing on the side of the photon detector. Sources were grounded with a thin graphite film.

A block diagram of the electronics is shown in Fig. 11. The output of the silicon detector was fed, through a short low-capacitance coaxial cable, to a low-noise Tennelec 100C* preamplifier. Identical Hamner N-383 linear amplifiers and Hamner N-685 differential discriminators with built-in variable delays were used in the two channels. The Hamner N-681 coincidence module was operated with a 70-nsec resolving time. The total number of $\beta$ particles in the energy window was recorded with a high counting-rate Hamner N-295 scaler. The coincidence circuit gated a Nuclear Data ND-120 512-channel analyzer in which the photon spectrum was recorded.

Electron-energy windows were chosen from 3 to 5 times as wide as the resolution of the electron detector. Drift of the $\beta$ energy window was $<2$ keV during any single run. A typical photon coincidence spectrum is shown in Fig. 12.

The following error sources were considered in computing the uncertainties in the measured probabilities: (a) statistical x-ray counting errors, (b) uncertainty in the shape of the continuum under the x-ray peak, (c) errors in solid-angle determination, (d) errors in the value of the fluorescence yield, (e) errors in the coincidence efficiency, (f) errors in the various absorption

[42] F. Suzor and G. Charpak, J. Phys. Radium **20**, 25 (1959).
[43] G. Charpak and F. Suzor, J. Phys. Radium **20**, 31 (1959).
[44] F. Suzor and G. Charpak, J. Phys. Radium **20**, 647 (1959).
[45] F. Suzor, J. Phys. Radium **21**, 223 (1960).

coefficients, and (g) errors in the escape-peak correction for $Pm^{147}$.

The lower-energy threshold of the $\beta$ channel was, in each case, sufficiently high so as to make the number of ejected orbital electrons above this threshold entirely negligible, compared with the number of $\beta$ particles counted.

With only a lower-energy threshold set in the $\beta$ channel, average $K$-shell excitation and ionization probabilities per $\beta$ decay were determined for three isotopes, with the following results:

$Y^{90}$: $P_K=(3.2\pm0.3)\times10^{-4}$ per $\beta$ for $E_\beta>624$ keV,
$Tc^{99}$: $P_K=(4.1\pm0.3)\times10^{-4}$ per $\beta$ for $E_\beta>70$ keV,
$Pm^{147}$: $P_K=(5.1\pm0.5)\times10^{-5}$ per $\beta$ for $E_\beta>70$ keV.

With the differential discriminator in the $\beta$ channel set to accept electrons in successive, rather narrow energy intervals, the probability, per $\beta$, of $K$-shell excitation and ionization was measured as a function of $\beta$ energy for $Tc^{99}$ and $Pm^{147}$. The results are presented in Figs. 13 and 14. The vertical error flags indicate standard deviations for the probabilities; the horizontal flags indicate the extent of each $\beta$-energy window. Results of the experiments described in Sec. III 2$A$ are also included in the figures.

The measurements reveal a strong $\beta$-energy dependence of the internal ionization probability; the probability decreases with increasing $\beta$ energy and vanishes for $E=E_0-I_K'$, where $E_0$ is the end-point energy of the $\beta$ spectrum and $I_K'$ is the $K$-shell ionization energy of the daughter atom. This $\beta$-energy dependence is in definite disagreement with the simple imperfect wave-function overlap theory [Eqs. (3) and (10)], which predicts a probability that is independent of $\beta$-particle energy. However, inclusion of phase-space factors in the imperfect wave-function overlap formalism [Eq. (14)] gives the proper shape, and use of antisymmetric relativistic wave functions leads to a prediction which is in quantitative agreement with the experimental results. The nonrelativistic wave-function calculations do not yield quantitative agreement. The $Y^{90}$ internal excitation and ionization probability for $E_\beta>624$ keV, reported above, and the total probability measured by Renard[46] (Table II), are in agreement with the internal-ionization modified shape factor $S$ given in Table I (see Fig. 4). Although the data for $Tc^{99}$ suggest that $S$ in this case has an allowed shape, further measurements at lower energies and a more definite calculation of $S$ would be desirable.

#### 4. Electron-Electron Coincidence Experiments

For the sake of completeness, we briefly summarize the results of published work on electron-electron coincidences performed on pure $\beta$ emitters. Such experiments have been carried out by Charpak, Suzor, and Spighel,[42–45,47] and by Duquesne,[48] and consist of measurements of the low-energy electron spectrum in coincidence with electrons above a given threshold energy, usually above the ionization energy of the $K$ shell. Compared with the predictions of the simple imperfect wave-function overlap theory, the measured spectra were more intense and decreased less rapidly with energy than expected. Furthermore, the intensities appeared to increase with atomic number[45] and the coincidence spectra showed an end-point energy roughly proportional to the end point of the $\beta$ spectrum.[48] When the second detector's energy window was moved up, a strong $\beta$-energy dependence of the ionization probability could be demonstrated,[47] especially for isotopes with low end-point energies.

Quantitative comparison of electron-electron coincidence results with theory is difficult because all atomic shells must be taken into account. Contributions from outer shells have been suggested as a possible reason for the discrepancy between experimental results and theoretical predictions based on imperfect wave-function overlap.[45] The direct-collision mechanism has been reexamined by Feinberg,[27] especially as it applies

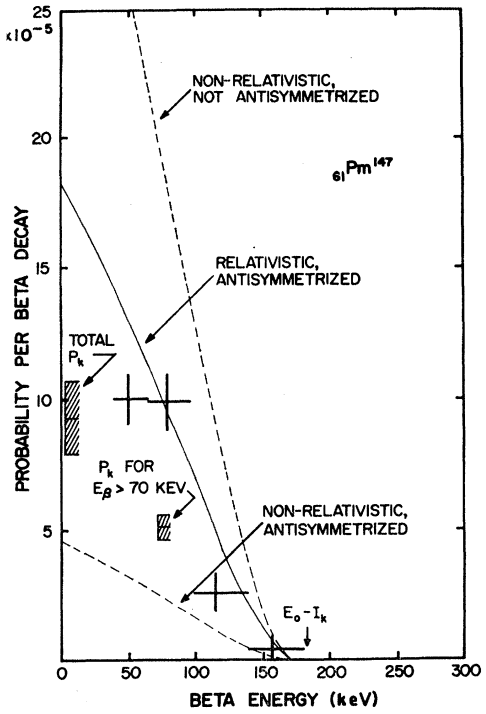


FIG. 14. Measured $K$-shell internal excitation and ionization probability in the $\beta$ decay of $Pm^{147}$, as a function of $\beta$-particle energy. Horizontal bars indicate $\beta$-energy window in coincidence measurements; vertical bars represent standard deviations. Cross-hatched vertical bars indicate measured total $K$-shell excitation and ionization probability associated with emission of $\beta$ particles above given energy. Curves are $K$-shell internal ionization probabilities calculated according to the modified imperfect wave-function overlap theory (Sec. II 2). Good agreement with experiment is obtained if relativistic wave functions are used in computing the transition matrix elements and the final-state wave function is antisymmetrized.

[46] G.-A. Renard, J. Phys. Radium **18**, 681 (1957).
[47] M. Spighel and F. Suzor, Nucl. Phys. **32**, 346 (1962).
[48] M. Duquesne, Ann. Phys. (Paris) **6**, 643 (1961).

to low-energy $\beta$ particles, for which it may dominate over the imperfect wave-function overlap mechanism. However, only partial agreement with the experimental electron-electron coincidence results could be attained. On the other hand, the electron-electron coincidence results are in qualitative agreement with the calculations reported in Sec. II 2, with the possible exception of the increase in ionization probability with $Z$.

## IV. CONCLUDING REMARKS

Clearly, further experiments on the interesting subject of the interactions between the atomic and nuclear parts of the atom during $\beta$ decay would be useful. Results of the present work on $\beta$-energy dependence of internal ionization, together with total internal ionization probabilities measured by others and by us, consitute a body of data that cannot be explained by the "direct-collision" mechanism nor by the traditional wave-function overlap theory. However, it has been shown here that the imperfect wave-function overlap theory can be improved by taking phase-space considerations into account, using relativistic electron wave functions in the calculation of the transition matrix elements, antisymmetrizing the final-state vector, and considering the allowed or forbidden character of the transitions. With these improvements, the theory agrees extremely well with available experimental results. The extent of the agreement is all the more surprising since only hydrogenic wave functions have been used and no screening corrections were made.

## ACKNOWLEDGMENTS

We are indebted to many colleagues for helpful conversations; in particular, we wish to thank I. E. McCarthy and R. L. Zimmerman. We are grateful to S. P. Granados for much technical help, and to V. O. Kostroun, who kindly checked some of the calculations. We thank A. G. Fowler of the University of British Columbia Computing Center for advice on programming.

PHYSICAL REVIEW VOLUME 164, NUMBER 4 20 DECEMBER 1967

# Prompt Neutron Emission from $U^{235}$ Fission Fragments

E. E. MASLIN, A. L. RODGERS, AND W. G. F. CORE
*United Kindgom Atomic Energy Authority, Aldermaston, Berkshire, England*
(Received 13 June 1967)

A description is given of measurements of the prompt neutron emission from fission fragments of $U^{235}$ in thermal neutron induced fission. A beam of neutrons from the AWRE research reactor HERALD induces fissions in a thin (20 $\mu$g/cm$^2$) sample of $U^{235}$. Neutrons are detected in a large (250 liters) liquid-scintillation counter and the fragment kinetic energies are measured with gold-silicon surface-barrier counters. Distributions, showing the neutron emission from both individual fission fragments and pairs of fragments, are given as functions of both the mass of the fragment and the total kinetic energy of the pair.

## 1. INTRODUCTION

PROMPT neutron emission from fission fragments provides valuable information relating to the energy balance in the fission process. The detailed shape of the curve connecting neutron emission with fragment mass number is believed to be connected directly[1,2] with the deformability of the fragments and in particular with the near-spherical shape of fragments containing numbers of neutrons and protons near to magic numbers, and indeed the deformability parameter for various nuclear species can be calculated directly from the experimental data.[2] The neutron emission from the fragments, considered as as indicator of the fragment excitation energy, is thus related more to the properties of the fragments than to the mass ratio of fragment division.

The most recent data for $U^{235}$ are those of Apalin *et al.*,[3] and of Milton and Fraser.[4] While agreement as to the general shape of the curve is obtained from these two sets of data, considerable divergencies exist as to the exact magnitude of the neutron emission ranging from 30% difference in regions of mass number 95 to approximately 70% for mass 155.

The main difficulties in this type of work relate to mass resolution, fragment coincident counting rate, and neutron-detection efficiency. While fragment time-of-flight techniques can provide the best mass resolution, they result in a low coincident counting rate, because of the small solid angle subtended at the source. Early measurements used ion chambers to measure the fragment energies. Surface-barrier counters have adequate energy resolution and can be close to the source but

[1] J. Terrell, Phys. Rev. **127**, 880 (1962).
[2] J. Terrell, in *Symposium of the Physics and Chemistry of Fission, 1965* (International Atomic Energy Agency, Vienna, 1965), Vol. 2, p. 3.
[3] V. F. Apalin, Yu. N. Gritsyuk, I. E. Kutikov, V. I. Lebedev, and L. A. Mikaelian, Nucl. Phys. **71**, 553 (1965).
[4] J. C. D. Milton and J. S. Fraser, in *Symposium on the Physics and Chemistry of Fission, 1965* (International Atomic Energy Agency, Vienna, 1965), Vol. 2, p. 39.